IEEE Access
Multidisciplinary ⋮ Rapid Review ⋮ Open Access Journal

Received June 15, 2020, accepted July 3, 2020, date of publication July 7, 2020, date of current version July 20, 2020.

Digital Object Identifier 10.1109/ACCESS.2020.3007678

New Algorithm to Discriminate Phase Distribution of Gas-Oil-Water Pipe Flow With Dual-Modality Wire-Mesh Sensor

FELIPE D. A. DIAS[1], EDUARDO N. DOS SANTOS[2,3], (Member, IEEE), MARCO J. DA SILVA[2,3], (Senior Member, IEEE), ECKHARD SCHLEICHER[1], RIGOBERTO E. M. MORALES[2], BUDDHIKA HEWAKANDAMBY[4], AND UWE HAMPEL[5]

[1]Institute of Fluid Dynamics, Helmholtz-Zentrum Dresden-Rossendorf, 01328 Dresden, Germany
[2]Multiphase Flow Research Center, Universidade Tecnológica Federal do Paraná, Curitiba 80230-901, Brazil
[3]Department of Electrical and Computer Engineering (CPGEI), Universidade Tecnológica Federal do Paraná, Curitiba 80230-901, Brazil
[4]Department of Chemical and Environmental Engineering, University of Nottingham, Nottingham NG7 2RD, U.K.
[5]Chair of Imaging Techniques in Energy and Process Engineering, Technische Universität Dresden, 01069 Dresden, Germany

Corresponding author: Felipe D. A. Dias (f.dias@hzdr.de)

This work was supported in part by the Royal Society, U.K., through the Newton Mobility under Grant NMG\R2\170169. The work of Felipe D. A. Dias was supported by the European Social Fund and the Free State of Saxony under Grant 100316833/100316834.

ABSTRACT Three-phase gas-oil-water flow is an important type of flow present in petroleum extraction and processing. This paper reports a novel threshold-based method to visualize and estimate the cross-sectional phase fraction of gas-oil-water mixtures. A 16 × 16 dual-modality wire-mesh sensor (WMS) was employed to simultaneously determine the conductive and capacitive components of the impedance of fluid. Then, both electrical parameters are used to classify readings of WMS into either pure substance (gas, oil or water) or two-phase oil-water mixtures (foam is neglected in this work). Since the wire-mesh sensor interrogates small regions of the flow domain, we assume that the three-phase mixture can be segmented according to the spatial sensor resolution (typically 2-3 mm). Hence, the proposed method simplifies a complex three-phase system in several segments of single or two-phase mixtures. In addition to flow visualization, the novel approach can also be applied to estimate quantitative volume fractions of flowing gas-oil-water mixtures. The proposed method was tested in a horizontal air-oil-water flow loop in different flow conditions. Experimental results suggest that the threshold-based method is able to capture transient three-phase flows with high temporal and spatial resolution even in the presence of water-oil dispersion regardless of the continuous phase.

INDEX TERMS Complex impedance, flow visualization, gas-oil-water horizontal flow, three-phase, wire-mesh sensor.

I. INTRODUCTION

Multiphase flows are widely found in many industrial processes. A typical example is gas-oil-water mixtures flowing simultaneously through production pipelines in the petroleum industry. The safe and efficient operation of processes involving multiphase flow requires advanced instrumentation to measure and visualize hydrodynamic flow parameters [1], [2]. Many measurement techniques have been proposed and tested in the past and have shown considerable progress in the monitoring of multiphase flows. However, measurement of three-phase gas-oil-water flow is still a challenge [2], [3]. Process tomography [4] emerged as non-intrusive approach for multiphase flow visualization. Conventional tomography systems, for example, x-ray [5], [6], gamma ray [7]–[10], electrical [11]–[14], optical [15]–[17], and ultrasound tomography [18]–[21], as well as MRI [22], [23], offer cross-sectional images of high temporal resolution but relatively low spatial resolution or vice-versa. For instance, radiation-based methods and MRI present high spatial resolution but are slow, thus being able to visualize only average structures. Electrical, optical and ultrasound tomography are fast but

The associate editor coordinating the review of this manuscript and approving it for publication was Zhigang Liu.

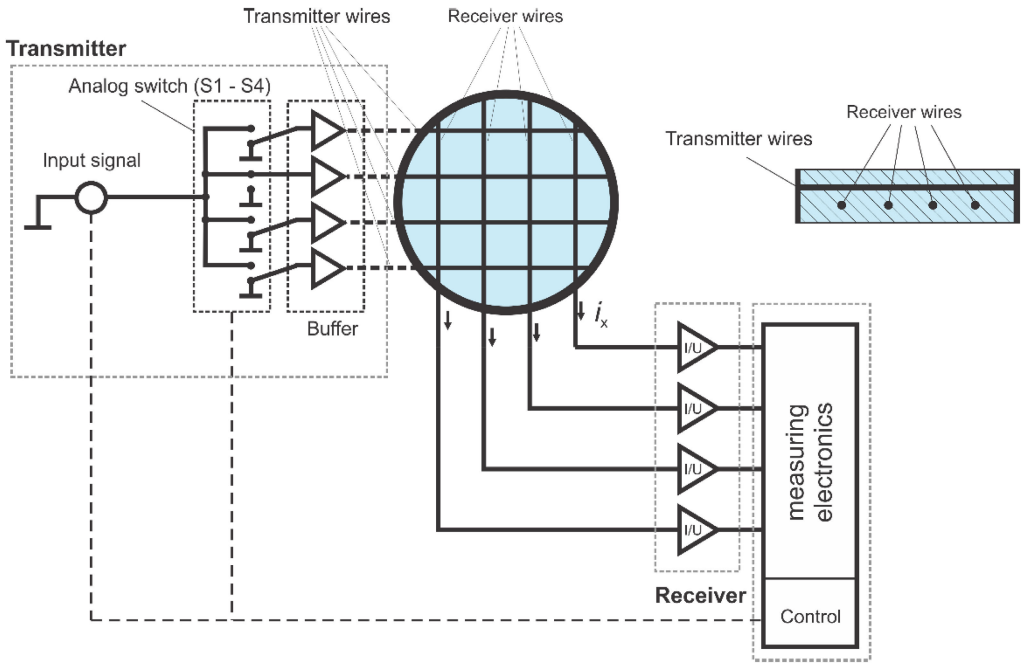

FIGURE 1. Wire-mesh sensor principle for a 4 × 4 electrodes configuration.

due to the diffusive nature of the signal carrier propagation, their spatial resolution is softer. More recently ultra-high-speed x-ray tomography [5], [6] has been introduced. It gives high speed and high spatial resolution but at the cost of high complexity. So far, most of the above techniques have been successfully applied only in two-phase gas-liquid flows.

A method similar to flow tomography uses a sensor proposed by [24] known as the wire-mesh sensor (WMS). It was initially proposed for air-water two-phase flow monitoring, but it has been improved over recent years to deal with non-conducting fluids [25], slurry flow [26] and three-phase flows [27], [28]. The method can be described as a hybrid solution between invasive local measurement of phase fraction and tomographic cross-sectional imaging. The sensor output provides two-dimensional images of the process with high temporal and spatial resolution.

In recent years, some efforts have been made by applying dual-modality measuring techniques for improving the range of application and in particular, to investigate three-phase gas-oil-water flows [29]–[31], in which two different sensing techniques are used to distinguish more than two substances. A proof of principle using dual-modality wire-mesh sensor based on complex permittivity measurements was introduced by [27] in which the measuring principle is based on simultaneous excitation at two distinct frequencies to interrogate each crossing point of a mesh sensor which in turn are linked to conductive and capacitive parts of fluid impedance. More recently, [28] presented a technique in order to discriminate fluids with different permittivity and conductivity values by measuring amplitude and phase circuit response from complex impedance measurement.

In this context, the dual-modality wire-mesh sensor measures the local conductivity and permittivity of multiphase fluids in several points over the cross-section pipe, being a so-called intrinsic and co-located dual-modality technique. Given the complex nature of gas-oil-water mixture, the dual-modality measurements (conductivity and permittivity) are not easily connected to phase fraction distribution. Hence, in this paper, we first review the measurement principle of amplitude and phase WMS and then discuss two data processing methods for obtaining phase distribution. The first was already applied in an earlier study [27] and a new threshold-based one is proposed here. Both methods are evaluated with experimental data from a three-phase flow facility.

II. DUAL MODALITY WIRE-MESH SENSOR

A. CURRENT STATE OF WIRE-MESH SENSOR TECHNOLOGY

The basic idea of a wire-mesh sensor is to span electrodes over the cross-section of a pipe in two adjacent axial planes whereby electrodes in each plane run parallel to each other. The electrodes of the one plane are used as transmitters and the electrodes of the other plane as receivers. Fig.1 shows the block diagram of the general electronics of a wire-mesh sensor for an exemplary sensor with 4 × 4 wires.

In the conductivity version [24], the transmitter wires are excited with bipolar signal pulses in successive order controlled by switches S1 to S4. The non-activated electrodes are connected to ground potential. The electrical current at a receiver wire resulting from the activation of a given transmitter wire is a measure of the conductivity of the fluid in

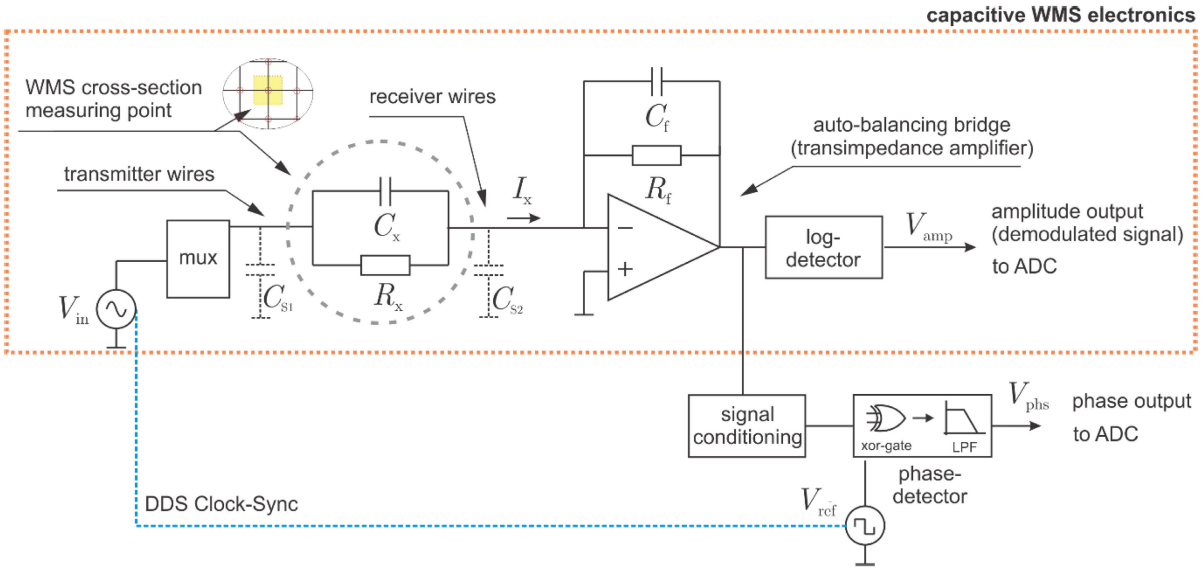

FIGURE 2. Electronics of capacitance wire-mesh sensor and new phase detection block. Signal generation is synchronized by the master clock of the Direct Digital Synthesizer (DDS).

the corresponding control volume close to the crossing point of the two wires. After activating the last transmitter wire, a complete set of measurements for the whole cross-section has been acquired. In this manner, the wire mesh subdivides the flow channel cross-section into a number of independent sub-regions, where each crossing point represents one sub-region. Each of the measured signals reflects the constitution of the flow within its associated sub-region, i.e. each crossing point acts as a local phase detector. Hence the set of data obtained from the sensor directly represents the phase distribution over the cross-section and no reconstruction procedure is needed in order to determine cross-sectional phase distributions, e.g. solving an inverse problem as usual in tomography. Recent investigations [32]–[34] show that the subdivision may have some overlap and introduce some reconstruction procedure for increasing resolution, however at increasingly computational cost and with too little improvement in the image quality.

In the capacitance version, a sinusoidal alternating voltage is employed for excitation and the receiver circuit must encompass a demodulator which converts the AC voltage into a proportional DC one. The sequential activation scheme for the transmitter wires and the parallel measurement of the receiver currents is the same as for the conductivity electronics [25].

As a step towards the further development of the wire-mesh sensor technology, recently developed dual-modality techniques are able to simultaneously determine the conductive and the capacitive components of the impedance of a fluid. The measuring principle is based on simultaneous excitation at two distinct frequencies. The acquisition is similar to the capacitance wire-mesh version, which converts the signals into a proportional voltage. However, in this case, the digitized amplitude signals are processed via the Fast Fourier Transform (FFT). Thus, based on amplitude measurements only and spectral analysis of measured data, the conductance and capacitance components of each crossing point can be determined [27]. However, this method works well only for low values of water conductivity (up to 100 μS/cm). Therefore, a new measuring topology was introduced in [28] and it is explained in detail bellow.

B. ELECTRONICS OF AMPLITUDE/PHASE WIRE-MESH SENSOR

In this work, we have modified the conventional capacitive WMS electronics [25], adding a phase detector block. Fig. 2 illustrates the electronics for one channel, i.e. considering one transmitter and one receiver wire (single crossing point). The standard capacitance wire-mesh sensor electronics is highlighted in orange, while the other block implements the phase detection scheme.

The sinusoidal excitation signal V_{in} (at typical 2 to 10 MHz frequency) is sequentially multiplexed to the transmitter electrodes. In the receiver path, the operational amplifier (opamp) converts the current I_{x} into a proportional AC voltage, which is fed to the log detector for signal demodulation (amplitude detection). The opamp output voltage signal is also fed into the phase detector block, which comprises a signal conditioning stage to convert the sinusoidal signal into a synchronized square-wave signal and a phase detector circuit. A XOR-gate and filtering is applied as a phase detector and requires an external reference square wave signal (phase-synchronized with the sinusoidal excitation signal) to measure the phase shift [35]. The output is an analog voltage that is proportional to the phase difference between the two signals. Both voltage signals carrying information on the amplitude V_{amp} and phase V_{phs} are fed into the A/D module of a standard WMS electronics.

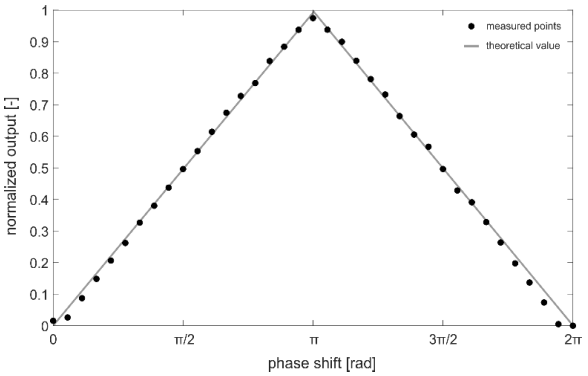

FIGURE 3. Transfer characteristic of the phase detector block.

The transfer theoretical and measured characteristics of the phase detector block are depicted in Fig. 3. The experimental data were obtained at a frequency of 10 MHz with a dual-output signal generator (AFG1022). The typical non-linearity of this type of circuit is seen at phase shifts of 0 and π (two-quadrant detector). Therefore, we usually place the initial phase shift at $\pi/2$ to obtain a linear response.

C. SIGNAL PROCESSING AND ELECTRICAL PROPERTIES OF FLUID ESTIMATION

In this section, we describe how to obtain the electrical properties of multiphase fluids from the measured amplitude and phase. For that we utilize the specific admittance $\mathbf{Y}$ as complex-value of fluid's electrical property in the form

$$\mathbf{Y} = \sigma + j\omega\varepsilon_0\varepsilon, \tag{1}$$

where $j = \sqrt{-1}$, $\varepsilon_0 = 8.85$ pF/m is the permittivity of free space, $\omega = 2\pi f$ is the angular frequency, f is the excitation frequency and the fluid properties are electrical conductivity σ and electrical relative permittivity ε.

The wire-mesh electronics acquires the amplitude V_{amp} and V_{phs} signals and stores the data into a 3D-matrix with size $X \times Y \times N$, (in this work we apply a 16×16 WMS, but this depends on the application) and N represents the acquired frames (i.e. acquisition period T times the frame rate FR). Prior to the experiments, two reference measurements are taken, i.e. the measurement with a substance of low permittivity (normally air) covering the whole sensor resulting in a reference data matrix for amplitude and phase. The process is repeated for a substance of high permittivity (normally tap water with known electrical conductivity). The temporal average is commonly used for amplitude and phase measurements. Hence, after this procedure, four 3D matrices V^H_{amp}, V^L_{amp}, V^H_{phs} and V^L_{phs} with size $X \times Y$ are obtained from

$$V^{\text{y}}_{\text{x}}(i,j) = \frac{1}{N}\sum_{k=0}^{N} V^{\text{y}}_{\text{x}}(i,j,k), \tag{2}$$

where x denotes the signal type (amp or phs) and y denotes the measurement at a high (H) or low (L) permittivity substance, further, i and j represent the spatial indexes and k the temporal index.

In the amplitude path (Fig. 3), the signal chain is the very same as for the standard capacitance wire-mesh sensor [36], which shows a logarithmic response given by

$$V_{\text{amp}} = V_{\text{a}} \cdot \ln\left(\frac{V_{\text{o}}}{V_{\text{b}}}\right), \tag{3}$$

where V_o is the linear amplitude at the operational amplifier output (Fig. 3) and the constants V_a and V_b are constants of the log-detector integrated circuit. It was shown that the measured amplitude V_{amp} is proportional to the modulus of the specific admittance $\mathbf{Y}$ (see [37], section 5.4.4) and can be written by following the same deductions but employing the modulus of the specific admittance instead of the pure relative permittivity as

$$V_{\text{amp}} = \text{a} \cdot \ln(|\mathbf{Y}|) + \text{b}, \tag{4}$$

where a and b are constants that encompass the sensor electronics, and the modulus of admittance is

$$|\mathbf{Y}| = \sqrt{\sigma^2 + (\omega\varepsilon_0\varepsilon)^2}. \tag{5}$$

Eventually, the constants a and b are defined pointwise as

$$\text{a}(i,j) = \frac{V^{\text{H}}_{\text{amp}}(i,j) - V^{\text{L}}_{\text{amp}}(i,j)}{\ln(|\mathbf{Y}^{\text{H}}|) - \ln(|\mathbf{Y}^{\text{L}}|)}, \tag{6}$$

$$\text{b}(i,j) = \frac{V^{\text{L}}_{\text{amp}}(i,j)\cdot\ln(|\mathbf{Y}^{\text{H}}|) - V^{\text{H}}_{\text{amp}}(i,j)\cdot\ln(|\mathbf{Y}^{\text{L}}|)}{\ln(|\mathbf{Y}^{\text{H}}|) - \ln(|\mathbf{Y}^{\text{L}}|)}. \tag{7}$$

Please, note that equations 6 and 7 are similar to the ones derived in [37], but here, the relative permittivity ε has been substituted by the modulus of specific admittance $|\mathbf{Y}|$. Thus, the modulus of the admittance for the high-value is given by

$$|\mathbf{Y}^{\text{H}}| = \sqrt{(\sigma^{\text{H}})^2 + (\omega\varepsilon_0\varepsilon^{\text{H}})^2}, \tag{8}$$

i.e. a scalar value, where σ^{H} is the electrical conductivity and ε^{H} the electrical relative permittivity of the substance, which usually is taken to be water. Typical values for water are $\sigma = 0.01$ S/m (100 μS/cm) and $\varepsilon = 80$ which at the excitation frequency of 10 MHz yields $|\mathbf{Y}^{\text{H}}| = 6.69\text{e-}2$ S. For $|\mathbf{Y}^{\text{L}}|$ the value at the given frequency is 5.56e-4 S. In this way, the measured value for each crossing point can be converted to the respective modulus of the admittance as

$$|\mathbf{Y}|(i,j,k) = \frac{V(i,j,k) - \text{b}(i,j)}{\text{a}(i,j)}. \tag{9}$$

As mentioned previously, the phase detector circuit is set to operate in a linear range. Therefore, the output voltage related to the phase lag can be written as

$$V_{\text{phs}}(i,j) = \text{c}(i,j)\cdot\phi(i,j) + \text{d}(i,j), \tag{10}$$

where ϕ is the phase lag of admittance $\mathbf{Y}$ defined as

$$\phi = \arctan\left(\frac{\omega\varepsilon_0\varepsilon}{\sigma}\right). \tag{11}$$

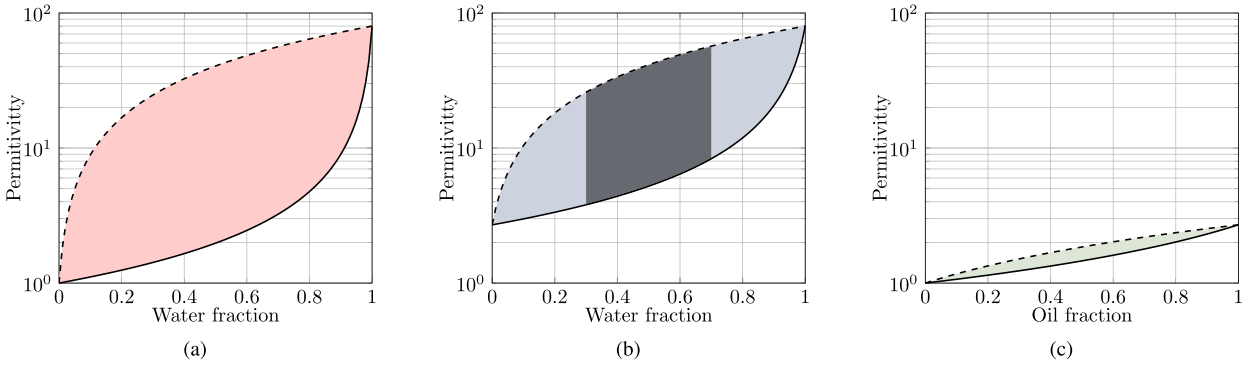

FIGURE 4. Effective permittivity of parallel (dashed-line) and series (continuous-line) model for two-phase mixtures. Coloured shading indicates all permittivity solutions bounded by parallel and series model. (a) Water-air (b) water-oil (gray shading represents possible inversion from water-oil dispersion) (c) oil-air mixture. Relative permittivity of water, oil and air are 80, 2.7 and 1, respectively.

Hence, from the reference measurements at the two know substances is possible to obtain the constants c and d in the form

$$\mathrm{c}(i,j) = \frac{V^{\mathrm{H}}(i,j) - V^{\mathrm{L}}(i,j)}{\phi^{\mathrm{H}} - \phi^{\mathrm{L}}}, \tag{12}$$

$$\mathrm{d}(i,j) = \frac{V^{\mathrm{L}}(i,j)\cdot\phi^{\mathrm{H}} - V^{\mathrm{H}}(i,j)\cdot\phi^{\mathrm{L}}}{\phi^{\mathrm{H}} - \phi^{\mathrm{L}}}. \tag{13}$$

The phase lag of air is $\phi^{\mathrm{L}} = \pi/2$ since the conductivity is zero and a typical value of the phase lag for water taking the values given previously is $\phi^{\mathrm{H}} = 0.7271$ rad $= 41.65$ deg. The measured phase lag is then given by

$$\phi(i,j,k) = \frac{V_{\mathrm{phs}}(i,j,k) - \beta(i,j)}{\alpha(i,j)}. \tag{14}$$

Finally, the complex-value admittance distribution can be obtained from

$$\mathbf{Y}(i,j,k) = Y(i,j,k)\cdot\exp(j\phi(i,j,k)), \tag{15}$$

and electrical permittivity and electrical conductivity distribution over time is calculated as

$$\varepsilon(i,j,k) = \mathrm{Im}\{\mathbf{Y}(i,j,k)\}\cdot(\omega\varepsilon_0)^{-1}, \tag{16}$$

$$\sigma(i,j,k) = \mathrm{Re}\{\mathbf{Y}(i,j,k)\}. \tag{17}$$

III. DATA PROCESSING

A. PHASE DISTRIBUTION DEPENDENCE

A typical impedance-based sensor relates the fluid phase (gas, oil water) fractions with the fluid's impedance. In most cases, this relationship also depends on how the phases are geometrically distributed in the interrogation region of the electrodes. Consequently, as well known, the measurement becomes flow regime dependent [38]. Fig. 4 shows the effective permittivity of two-phase mixtures based on two models: parallel and series, which are known as Wiener bounds [39],

$$\varepsilon_{\mathrm{parallel}} = (\varepsilon_2 - \varepsilon_1)\alpha + \varepsilon_1, \tag{18}$$

$$\varepsilon_{\mathrm{series}} = \frac{\varepsilon_1\varepsilon_2}{(\varepsilon_2 - \varepsilon_1)\alpha + \varepsilon_1}, \tag{19}$$

where ε_1 and ε_2 are the relative permittivity of two pure substances and α is the volume fraction of component 1. Both parallel and series models (18), (19) delimit the upper and lower boundaries for a standard capacitance sensor as long as the mixture has negligible dielectric losses. Hence, any phase distribution combination of two-phase flows should be within the area limited by the boundaries. Note that the greater the permittivity difference between two components, the greater the area between upper and lower boundaries and consequently, the greater the dependence on geometrical factors (i.e. flow regime).

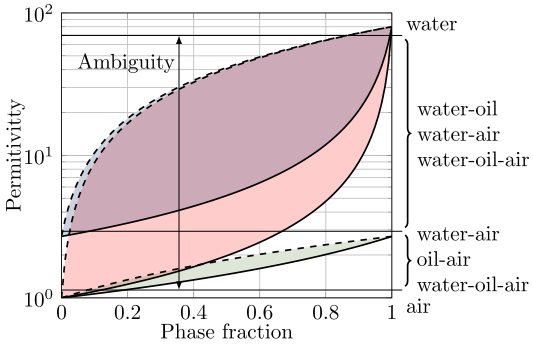

FIGURE 5. Indetermination of effective permittivity of three-phase mixture based on parallel and series two-phase mixture model. The X-axis is water fraction for water-air (pink area) and water-oil (blue area) mixtures and oil fraction for the oil-air mixture (green area). The purple area represents an intersection of water-oil and water-air mixtures.

B. CONTINUOUS PHASE INVERSION

In addition to the dependence on geometrical factors, oil-water mixtures can stream in the form of oil-in-water (water continuous) or water-in-oil (oil continuous) dispersion depending on the flow conditions. Fig. 4b depicts the limits of a possible phase inversion assuming it may be formed with up to 80% of the dispersed phase. In this way, if only permittivity information is available, one cannot distinguish continuous and dispersed phases. This issue is even more challenging for water-oil-air three-phase mixtures. As shown in Fig. 5, a large

range of effective permittivity is undetermined, except in two small regions on top and bottom, when the sensor is filled up with the lowest and highest permittivity components. Such conclusions have also been shown elsewhere [40].

In order to deal with the above-mentioned indetermination and flow regime dependence, many researchers have applied mixture models based on different assumptions, for instance the parallel model [41], the expanded Maxwell-Model for three phase [27] and more recently the Maxwell model for air-water flows [42].

In the scope of dual-modality impedance-based sensors, it seems reasonable to use models that relates the real and imaginary parts of the complex impedance of the mixture, for instance Van Beek's model [43]. In this approach, the equivalent specific complex admittance eq. (1) for the two-phase mixture is approximated as a continuous phase containing small spheres of a second component. The mathematical model is:

$$\begin{aligned} \mathbf{Y}_{\mathrm{m}} &= \mathbf{Y}_1 \frac{2\mathbf{Y}_1 + \mathbf{Y}_2 + 2\alpha_2(\mathbf{Y}_2 - \mathbf{Y}_1)}{2\mathbf{Y}_1 + \mathbf{Y}_2 - \alpha_2(\mathbf{Y}_2 - \mathbf{Y}_1)}, \\ \alpha_1 &= 1 - \alpha_2 \end{aligned} \tag{20}$$

Index 1 and 2 represent the continuous and dispersed phases, respectively and α the volume fraction. In flow conditions where the interfaces can be approximated by (20), the area representing the phase distribution dependency is reduced to single lines, as depicted in Fig. 6.

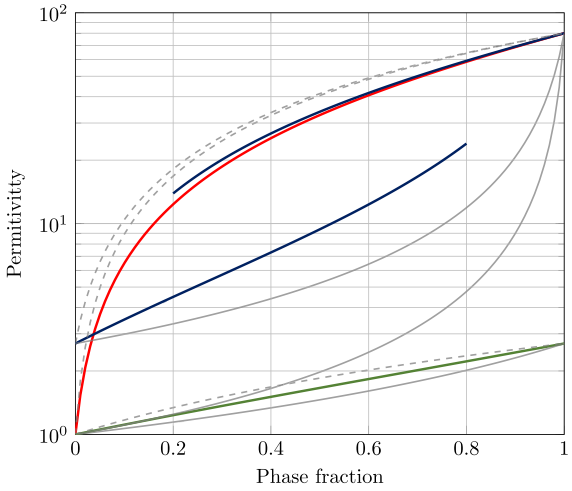

FIGURE 6. Van Beek's model [43]. Water-air (red); water-oil (blue) oil-air (green). Parallel and series models in gray. The X-axis is the phase fraction of the component water in water-air and water-oil mixtures and oil in the oil-air mixture.

Dykesteen *et al.* [44] proposed an extension for three-phase mixtures using the same assumptions:

$$\begin{aligned} \mathbf{Y}_{\mathrm{m}} &= \mathbf{Y}_1 \frac{\mathbf{Y}_1(1 + 2x)}{(1 - x)}, \\ x &= \alpha_2 \frac{(\mathbf{Y}_2 - \mathbf{Y}_1)}{(\mathbf{Y}_2 - 2\mathbf{Y}_1)} + \alpha_3 \frac{(\mathbf{Y}_3 - \mathbf{Y}_1)}{(\mathbf{Y}_3 - 2\mathbf{Y}_1)}. \end{aligned} \tag{21}$$

Based on (21), Dos Santos *et al.* [27] formulated the direct and inverse problem to fuse data from a dual-modality wire-mesh sensor. Since we will compare this approach to a newly proposed one, the inverse problem is shown below. For more details, the reader is referred to [27]. The phase fraction of water-oil-air three-phase flow is estimated as

$$\mathbf{x} = \mathbf{A}^{-1}\mathbf{b}. \tag{22}$$

Here, $\mathbf{A}$ and $\mathbf{b}$ are

$$\begin{aligned} \mathbf{A} &= \begin{bmatrix} 0 & a_{12} & a_{13} \\ 0 & a_{22} & a_{23} \\ 1 & 1 & 1 \end{bmatrix}, \\ a_{12} &= 2\sigma_1\sigma_b - 2k^2\varepsilon_1\varepsilon_b + \sigma_b\sigma_{\mathrm{m}} - k^2\varepsilon_b\varepsilon_{\mathrm{m}} \\ a_{13} &= 2\sigma_1\sigma_c - 2k^2\varepsilon_1\varepsilon_c + \sigma_c\sigma_{\mathrm{m}} - k^2\varepsilon_c\varepsilon_{\mathrm{m}} \\ a_{22} &= 2\varepsilon_1\sigma_b + 2\sigma_1\varepsilon_b + \varepsilon_b\sigma_{\mathrm{m}} + \sigma_b\varepsilon_{\mathrm{m}} \\ a_{23} &= 2\varepsilon_1\sigma_c + 2\sigma_1\varepsilon_c + \varepsilon_c\sigma_{\mathrm{m}} + \sigma_c\varepsilon_{\mathrm{m}} \end{aligned} \tag{23}$$

and

$$\begin{aligned} \mathbf{b} &= \begin{bmatrix} b_1 & b_2 & 1 \end{bmatrix}^{\mathrm{T}}. \\ b_1 &= \sigma_{\mathrm{m}}\sigma_a - k^2\varepsilon_{\mathrm{m}}\varepsilon_a - \sigma_1\sigma_a + k^2\varepsilon_1\varepsilon_a \\ b_2 &= \varepsilon_{\mathrm{m}}\sigma_a + \sigma_{\mathrm{m}}\varepsilon_a - \varepsilon_1\sigma_a - \sigma_1\varepsilon_a \end{aligned} \tag{24}$$

The continuous phase is found assuming a threshold value of 10% of the conductivity of water. Results of static and dynamic experiments upon lab conditions were presented in [27], showing the method has a high potential. However, the system might be unstable depending on the flow conditions. Although the matrix $\mathbf{A}$ is well-posed and has a unique solution, it presents very small singular values for water-oil-air mixtures. Therefore, noise and modeling error could generate physical inconsistency on the phase distribution. As an alternative, we propose a novel threshold-based method to overcome instability generated by the inverse problem.

C. THRESHOLD-BASED METHOD FOR THREE-PHASE FLOW VISUALIZATION

The method proposed in this paper consists of classifying wire-mesh sensor data of water-oil-air three-phase flow. Each local measurement is divided into five categories: 1) water; 2) oil in water (o/w) dispersion; 3) water in oil (w/o) dispersion; 4) oil; and 5) gas. The classification is performed by relating local conductivity and permittivity of the mixture acquired from a dual-modality wire-mesh sensor.

1) TWO-PHASE MIXTURE APPROXIMATION

In order to deal with the above-discussed ambiguity of phase distribution determination from the mixture electrical properties (Fig. 5), we assume that the interrogating volume between transmitter and receiver wires of a single crossing-point is small enough to be approximated as either a single phase or a two-phase mixture instead of three-phase mixture. Fig. 7 illustrates this concept for a water continuous example, but it may be extrapolated to other cases. As shown in Fig. 7a, if we assume a simple impedance probe that interrogates the

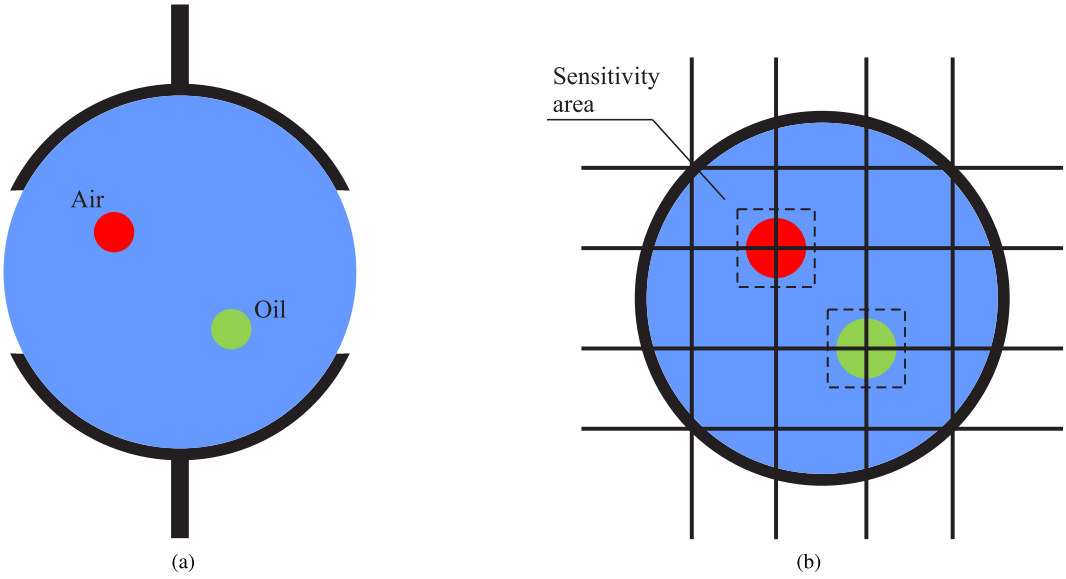

FIGURE 7. Three-phase mixture with water continuous phase containing oil and air dispersed phase. (a) Two plates capacitor (b) wire-mesh sensor; dashed box represents an ideal sensitivity area of WMS crossing-point.

whole cross section of a pipe, the substance between the electrodes is seen as a three-phase mixture, where water is the continuous and oil and air are the dispersed phases. Ideally, Dykesteen's model [44] (Eq. 21) would be able to determine the phase fractions from impedance (admittance) measurements. However, as already said, this model becomes unstable for many practical situations, even when applied to WMS. In this work, instead, since the wire-mesh sensor interrogates small regions of the flow, we assume that the three-phase mixture can be segmented according to the spatial sensor resolution (typically 2-3 mm). In Fig. 7b, for example, air and oil phases located at the regions 1 and 2 can be detected by the respective crossing-points even if there is a small portion of the continuous phase. The goal of this approach is to simplify a complex three-phase system as several local two-phase mixtures in order to avoid ambiguity between combinations of the mixture with equivalent permittivity. We summarize the assumptions below:

a) The content of each WMS crossing-point is approximated as single phase or two-phase mixture, i.e. each local measurement is divided into five categories: (1) water; (2) oil in water (o/w) dispersion; (3) water in oil (w/o) dispersion; (4) oil; and (5) gas;
b) Foam, gas-oil and gas-water mixtures are not considered. Thus, low permittivity mixtures will be classified as pure gas;
c) Continuous phase inversion of water/oil dispersion (either o/w or w/o) can be identified assuming a threshold value of 10% water conductivity [27], i.e. an electrically conducting dispersion is water continuous and an electrically non-conducting dispersion is oil continuous.
d) Water-oil dispersion may occur with the continuous phase ranging up to 80% phase fraction in either case (i.e. o/w or w/o dispersion) [38].

Hence, in order to classify all segmented regions, a thresholding and decision approach is applied. Algorithm 1 summarizes the decision process. The definition of the threshold values is detailed below.

2) THRESHOLD SELECTION

Taking into account the assumptions discussed previously, we can use van Beek's model [43] as a start point to define threshold values for multiphase flow visualization. The first threshold T_σ is employed to split Eq. (20) into electrically conductive and non-conductive parts (assumption c). Fig. 8a and 8b shows the solution in terms of effective permittivity assuming that T_σ is 10% of the water conductivity. The gray lines represent all possible solutions without constraints, which in turn cause indeterminacy. However, if we assume that the gas phase covers almost the entire sensitivity area of a single crossing-point (as in Fig. 7b) and dispersion has up to 80% of the dispersed phase (assumption d), there is no combination of mixture overlapping each other. Here, we can finally define thresholds based on permittivity to classify the type of mixture for individual crossing-points. If the mixture is conductive, T_w classifies the mixture in two groups: water or oil-in-water dispersion (o/w) (Fig. 8a). For non-conductive fluids, $T_{(w/o)}$ and T_g classify the components as water-in-oil dispersion (w/o), oil or gas (Fig. 8b). According to assumption b, T_g is defined as not to consider gas/oil mixtures. It is important to note that water and oil do not mean pure phases, but an interval with a high content of the given substance. Table 1 summarizes the five intervals and thresholds based on van Beek's model and decision process of Algorithm 1.

3) THREE-PHASE FLOW VISUALIZATION

Based on Table 1, each crossing-point (i, j) is classified according to the permittivity and conductivity of the mixture.

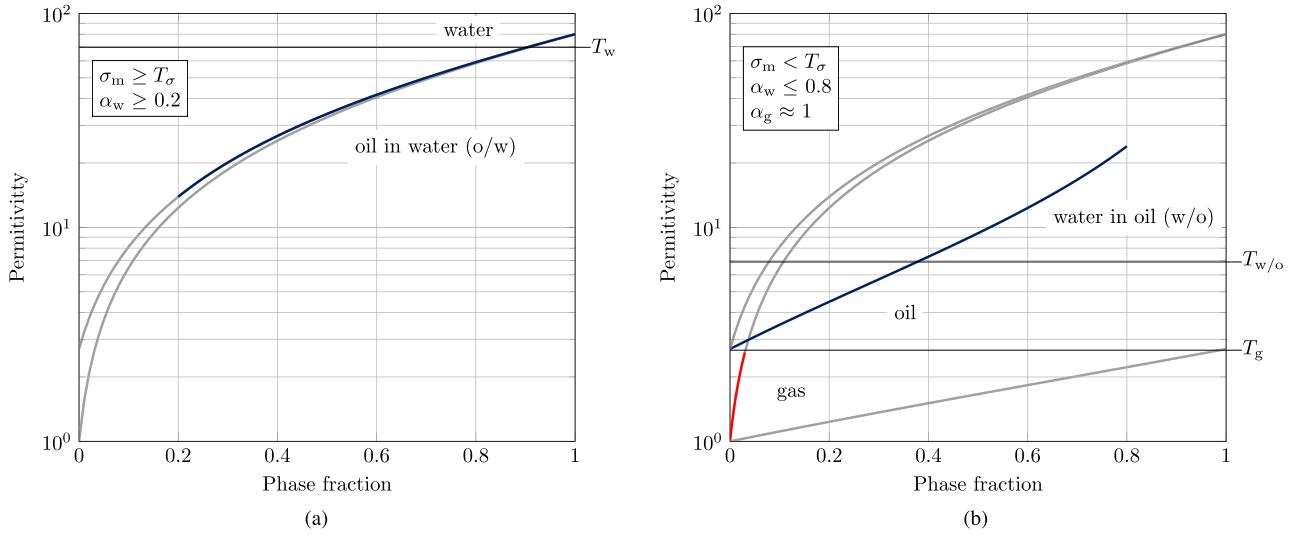

FIGURE 8. Effective permittivity based on van Beek's model [43]. Gray lines indicates all solutions without constraints. (a) Solution subject to conductivity greater than 10% of water conductivity and water continuous phase up to 20%. Oil in water dispersion in blue (o/w); (b) Solution for non-conductive mixtures. Water in oil dispersion (w/o) also in blue. Air (red) represents 96% of air in water-air mixture and 100% air of oil-air mixture.

TABLE 1. Phase fraction range of five types of mixtures based on van Beek's model [43].

Classification	Phase fraction					Threshold	Permittivity
	Water		Oil		Gas		
x	$\alpha^{w}_{x,min}$	$\alpha^{w}_{x,max}$	$\alpha^{o}_{x,min}$	$\alpha^{o}_{x,max}$	α^{g}_{x}	T_x	ε_x
Water (w)	0.9	1	0	0.1	0	T_w	70
Oil-in-water dispersion (o/w)	0.2	0.9	0.1	0.8	0		
Water-in-oil dispersion (w/o)	0.4	0.8	0.2	0.6	0	$T_{w/o}$	9
Oil (o)	0	0.4	0.6	1	0		
Air (g)	0	0	0	0	1	T_g	2.7

Algorithm 1 Threshold-Based Method

```
if σ_m ≥ 0.1σ_w then
    if ε_m ≥ T_w then
        "Water"
    else
        "Oil in water dispersion"
    end if
else if σ_m < 0.1σ_w then
    if ε_m ≥ T_w/o then
        "Water in oil dispersion"
    else if T_w/o > ε_m ≥ T_g then
        "Oil"
    else
        "Air"
    end if
end if
```

If $\sigma_m \geq T_\sigma$, the local volume fraction interval is defined as:

$$\mathbf{A}_w(i,j,k) = \begin{cases} 1, & \text{if } \varepsilon_m(i,j,k) \geq T_w, \\ 0, & \text{otherwise.} \end{cases} \tag{25}$$

$$\mathbf{A}_{o/w}(i,j,k) = \begin{cases} 1, & \text{if } \varepsilon_m(i,j,k) < T_w, \\ 0, & \text{otherwise.} \end{cases} \tag{26}$$

If $\sigma_m < T_\sigma$, then

$$\mathbf{A}_{w/o}(i,j,k) = \begin{cases} 1, & \text{if } \varepsilon_m(i,j,k) \geq T_{w/o}, \\ 0, & \text{otherwise.} \end{cases} \tag{27}$$

$$\mathbf{A}_o(i,j,k) = \begin{cases} 1, & \text{if } T_{w/o} > \varepsilon_m(i,j,k) > T_g, \\ 0, & \text{otherwise.} \end{cases} \tag{28}$$

$$\mathbf{A}_g(i,j,k) = \begin{cases} 1, & \text{if } \varepsilon_m(i,j,k) < T_g, \\ 0, & \text{otherwise.} \end{cases} \tag{29}$$

Note that $\mathbf{A}_x$ is a 3D binary matrix which can be used to generate images from the pipe cross-section. It can be done by encoding all five 3D matrix in RGB scale as follows:

$$\begin{aligned} \mathbf{A}_{red} &= \sum_x r_x \cdot \mathbf{A}_x, \\ \mathbf{A}_{green} &= \sum_x g_x \cdot \mathbf{A}_x, \\ \mathbf{A}_{blue} &= \sum_x b_x \cdot \mathbf{A}_x, \end{aligned} \tag{30}$$

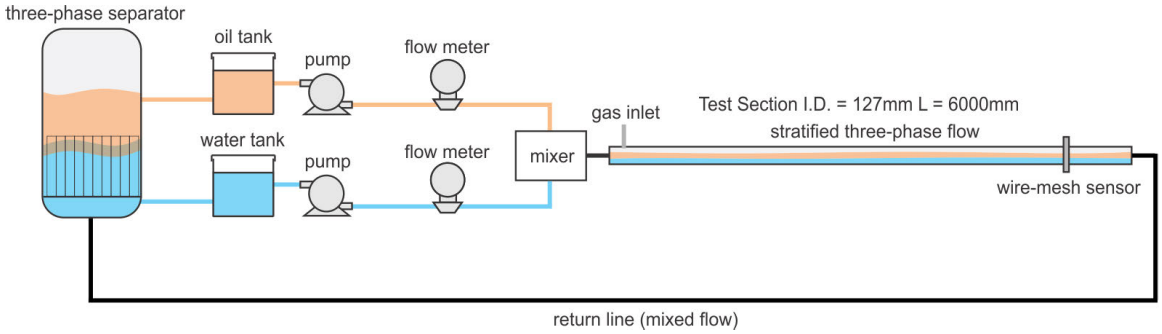

FIGURE 9. Schematic diagram of the three-phase flow experimental loop.

TABLE 2. RGB color codification.

Classification (x)	r	g	b	Color
Water (w)	0	0	255	
Oil in water (o/w)	0	180	255	
water in oil (w/o)	0	100	0	
Oil (o)	255	255	0	
Gas (g)	255	0	0	

TABLE 3. Liquid substances properties.

Property	Tap water	Silicone oil
Density ρ [kg/m^3]	998	916
Viscosity η [kg/m.s]	0.001	0.0052
Electrical Conductivity σ [μS/cm]	500	-
Electrical Permittivity ε [-]	79.8	2.7

where x represents the classification of mixture and r, g and b are the weights for each color, as summarized in Table 2.

4) QUANTITATIVE VOLUME PHASE FRACTION ESTIMATION

The novel approach introduced may not only show images of the pipe flow, but also be applied to estimate the minimum and maximum oil and water volume fractions. The rationale here is not to find the exact volume fraction as by solving an inverse problem [27], but to identify the boundaries of each classified reading in order to evaluate it quantitatively. Hence, we take the values from Table 1 to calculate the boundaries, as is detailed below.

Firstly, the time series of each interval is obtained by averaging the matrices (25) to (29) as

$$\mathbf{A}_{\mathrm{x}}(k) = \sum_i \sum_j a_{i,j} \cdot \mathbf{A}_{\mathrm{x}}(i,j,k), \tag{31}$$

where $a_{i,j}$ is a weight matrix to consider the shape of the pipe [45]. By time-averaging (31) as

$$\overline{\alpha}_{\mathrm{x}} = \frac{1}{N} \sum_{k=1}^{N} \mathbf{A}_{\mathrm{x}}(k), \tag{32}$$

one gets a scalar value that represents the area- and time-average phase fraction of a given experiment. Since we have assumed there is no foam in the process, we can estimate liquid fraction by:

$$\overline{\alpha}_{\mathrm{liquid}} = \overline{\alpha}_{\mathrm{w}} + \overline{\alpha}_{\mathrm{o/w}} + \overline{\alpha}_{\mathrm{w/o}} + \overline{\alpha}_{\mathrm{o}}, \tag{33}$$

and due to the continuity equation, hence

$$\overline{\alpha}_{\mathrm{gas}} = 1 - \overline{\alpha}_{\mathrm{liquid}}. \tag{34}$$

The boundaries for the phase fractions are obtained taking the values from Table 1. Note that due to the continuity equation, if the maximal value for water fraction is assumed, then the minimal value for oil is taken, and vice versa:

$$\alpha^{\mathrm{w}}_{\mathrm{x,min}} + \alpha^{\mathrm{o}}_{\mathrm{x,max}} = \alpha^{\mathrm{w}}_{\mathrm{x,max}} + \alpha^{\mathrm{o}}_{\mathrm{x,min}} = \overline{\alpha}_{\mathrm{liquid}}. \tag{35}$$

Thus, the boundaries can be finally calculated as follows:

$$\begin{aligned}\overline{\alpha}_{\mathrm{w,min}} &= (\alpha^{\mathrm{w}}_{\mathrm{w,min}}) \cdot \overline{\alpha}_{\mathrm{w}} + (\alpha^{\mathrm{w}}_{\mathrm{o/w,min}}) \cdot \overline{\alpha}_{\mathrm{o/w}} \\ &\quad + (\alpha^{\mathrm{w}}_{\mathrm{w/o,min}}) \cdot \overline{\alpha}_{\mathrm{w/o}} + (\alpha^{\mathrm{w}}_{\mathrm{o,min}}) \cdot \overline{\alpha}_{\mathrm{o}}, \end{aligned} \tag{36}$$

$$\begin{aligned}\overline{\alpha}_{\mathrm{o,max}} &= (1 - \alpha^{\mathrm{w}}_{\mathrm{w,min}}) \cdot \overline{\alpha}_{\mathrm{w}} + (1 - \alpha^{\mathrm{w}}_{\mathrm{o/w,min}}) \cdot \overline{\alpha}_{\mathrm{o/w}} \\ &\quad + (1 - \alpha^{\mathrm{w}}_{\mathrm{w/o,min}}) \cdot \overline{\alpha}_{\mathrm{w/o}} + (1 - \alpha^{\mathrm{w}}_{\mathrm{o,min}}) \cdot \overline{\alpha}_{\mathrm{o}}, \end{aligned} \tag{37}$$

and

$$\begin{aligned}\overline{\alpha}_{\mathrm{w,max}} &= (\alpha^{\mathrm{w}}_{\mathrm{w,max}}) \cdot \overline{\alpha}_{\mathrm{w}} + (\alpha^{\mathrm{w}}_{\mathrm{o/w,max}}) \cdot \overline{\alpha}_{\mathrm{o/w}} \\ &\quad + (\alpha^{\mathrm{w}}_{\mathrm{w/o,max}}) \cdot \overline{\alpha}_{\mathrm{w/o}} + (\alpha^{\mathrm{w}}_{\mathrm{o,max}}) \cdot \overline{\alpha}_{\mathrm{o}}, \end{aligned} \tag{38}$$

$$\begin{aligned}\overline{\alpha}_{\mathrm{o,min}} &= (1 - \alpha^{\mathrm{w}}_{\mathrm{w,max}}) \cdot \overline{\alpha}_{\mathrm{w}} + (1 - \alpha^{\mathrm{w}}_{\mathrm{o/w,max}}) \cdot \overline{\alpha}_{\mathrm{o/w}} \\ &\quad + (1 - \alpha^{\mathrm{w}}_{\mathrm{w/o,max}}) \cdot \overline{\alpha}_{\mathrm{w/o}} + (1 - \alpha^{\mathrm{w}}_{\mathrm{o,max}}) \cdot \overline{\alpha}_{\mathrm{o}}. \end{aligned} \tag{39}$$

IV. EXPERIMENTAL METHODOLOGY

A. FLOW LOOP

The University of Nottingham multiphase flow laboratory is equipped with a flow loop designed to test liquid-liquid two-phase flow [46]. However, it is possible to adjust the system to introduce a gas phase to perform stratified three-phase flow measurements as a proof of concept. The flow loop, illustrated in Fig. 9, is composed of water and silicon oil storage tanks with a capacity of 4.87 m^3 each (see Table 3 for substances properties). Two pumps supply the liquid phases into the system, and the flow rate is measured using an electromagnetic flow meter for water and a turbine flow

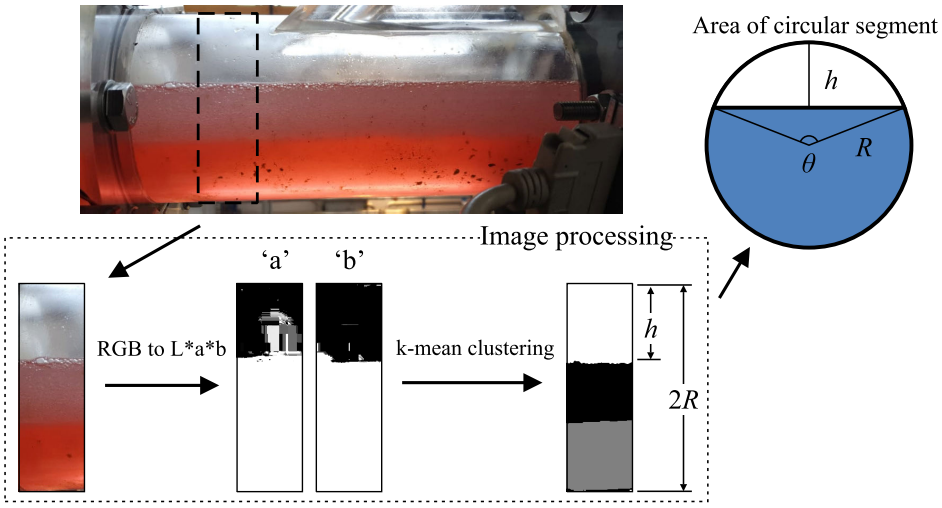

FIGURE 10. Image-processing to obtain gas fraction references.

meter for silicon oil. The oil and water inlets are connected to a specially designed static homogenizer with a flexible hose, where the fluids are pre-mixed before the mixture flows into the test section. This arrangement is chosen to ensure that any dispersion created was caused by the hydrodynamics of the flow rather than any mixing effects. For qualitative experiments, gas can be injected downstream the water-oil mixer with pressure up to 6 bar, but due to facility restrictions, the gas flow rate was not monitored. Nevertheless, three-phase flow is generated, and reference phase fractions were estimated as will be described in sections below. The test section consists of a sudden pipe expansion from an internal diameter of 50.8 mm × 2000 mm long to 127 mm × 6000 mm long. The experimental test section was set at the far end of the experimental circuit to investigate properly the three-phase flow interfaces. The output stream goes to a cylindrical stainless-steel vessel for separation of the two-phase mixture of silicone oil and water placed in a vertical position. The separator vessel has dimensions of 2.438 m I.D. × 2.438 m height, containing coalesce cartridges, manufactured by Knitmesh Ltd.

Measurements were performed with a 16 × 16 wire-mesh sensor connected to a pipe segment. In order to obtain the reference values, measurements were taken with the pipe section empty and fully filled with water, prior to the experiments. In this test, nine experimental conditions were defined with gas flow rate set to zero (see Table 4). A final experiment (P10) was performed to check the capability of WMS to capture transient three-phase flows. Thus, gas was injected into the flow loop with a constant pressure of 6 bar in order to generate slug flow. Each measurement consists of 120 seconds long at 1000 frames per seconds. The data set used in this work are available on [47].

B. IMAGE-BASED AIR VOLUME DETECTION

In order to evaluate quantitatively the experimental data, gas-liquid interfaces were extracted from pictures of a transparent section of the pipeline based on the color classification algorithm. In this way, red dye was added to the water to increase the colour contrast between the phases. As depicted in Fig. 10, individual frames were converted from RGB to L*a*b colour space, classified using k-means clustering and finally, segmented in three colours (see [48], section 13).

TABLE 4. Experimental flow conditions.

Experimental point	Water flow rate [m^3/h]	Oil flow rate [m^3/h]
P1	1.68	1.05
P2	1.71	5.06
P3	2.16	10.96
P4	9.31	1.43
P5	9.20	5.24
P6	9.62	10.13
P7	17.41	1.72
P8	16.52	5.42
P9	16.57	10.65
P10 (slug flow)	15.90 and 25.12 (after 45 s)	9.22 and 0 (after 45 s)

Since the photo captures only the lateral view of the pipe, the area of the circular section covered by gas is estimated relating the pipe radius R to the measured vertical gas height h as:

$$\theta = 2\cos^{-1}\left(1 - \frac{h}{R}\right). \tag{40}$$

Thus, the area occupied by the gas is

$$A_{sc}(k) = \frac{R^2}{2}(\theta - \sin\theta), \tag{41}$$

and the (reference) image-based gas fraction is obtained from

$$\overline{\alpha}_{\text{gas,ref}} = \frac{A_{sc}}{A}, \tag{42}$$

where A is the pipe area.

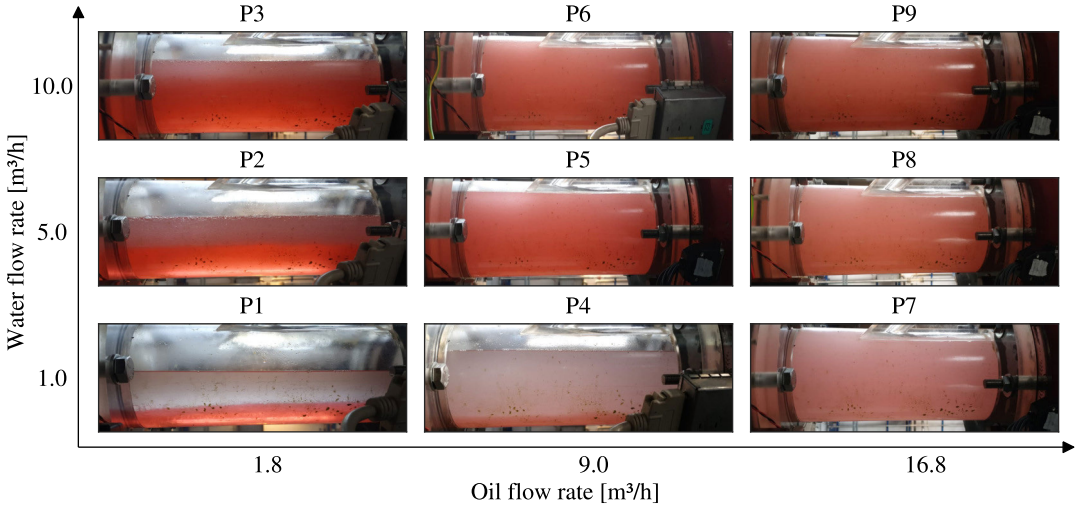

FIGURE 11. Slide view images of all operating points that will be compared with WMS data.

C. REFERENCE OIL AND WATER VOLUME FRACTIONS

By applying the continuity equation on (42), we find the liquid fraction

$$\overline{\alpha}_{\text{liquid,ref}} = \overline{\alpha}_{\text{gas,ref}}. \tag{43}$$

It is reasonable to assume no-slip condition between water and oil in order to yield an estimate of the phase fractions for oil and water. Hence, we can finally estimate water and oil fraction references as

$$\overline{\alpha}_{\text{water,ref}} = \frac{Q_{\text{water,in}}}{Q_{\text{liquid,in}}} \cdot \overline{\alpha}_{\text{liquid,ref}}, \tag{44}$$

$$\overline{\alpha}_{\text{oil,ref}} = \frac{Q_{\text{oil,in}}}{Q_{\text{liquid,in}}} \cdot \overline{\alpha}_{\text{liquid,ref}}. \tag{45}$$

where, Q_x is the average flow rate injected into the system (Table 4).

V. RESULTS

A. OVERVIEW

Dual modality wire-mesh sensor data were acquired and processed to visualize cross-sectional air-oil-water three-phase flow. Fig. 11 summarizes the nine flow conditions investigated. Fig. 12a and Fig. 12b depicts the cross-sectional images of the same points generated from dual-modality WMS, where the first one was performed based on the novel threshold-based method and the second one by the inverse problem formulation [27]. By observation, it is clear that the threshold method can capture fine details of the flow, i.e. gas-in-liquid interfaces, occurrence of dispersion and accumulation of water on the bottom of the pipe. On the other hand, the inverse problem presented poor solutions for most of the operating points, since the ambiguity caused by air and oil has not been treated. Only for well-separated flows, it has presented results (i.e. operating points P1, P2 and P3).

B. QUALITATIVE RESULTS

Fig. 13 depicts the experimental points P1 and P2 and compares both methods against an image of the pipe. In this case, the oil flow rate kept constant for both experiments while the water flow rate is increased. The individual phase fractions stream mostly separated in P1 (Fig. 13b). In P2 (Fig. 13a), high content of water flows on the bottom of the pipe, while water-oil dispersion streams between water and gas interfaces. It can be seen that both methods were able to capture water, oil and air interfaces. However, according to the reference images, the inverse problem inferred as air-water mixture a few pixels with no presence of air (pink/purple pixels). In addition, the phase fraction estimation is clearly incorrect, since in both operating points, water and oil fractions were valued as pure substances. In contrast, the threshold-based method showed no ambiguity between air and oil as discussed earlier. The dispersion phases also seem to be correct in the operating point P2 (Fig. 13a).

Fig. 14 shows the points P5 and P8, where the water flow rate is constant and oil flow rate is varied. By observation, it is not possible to quantify the concentration of continuous and dispersed phase of water-oil dispersion, but we can evaluate the capability of both methods to deal with the ambiguity between non-conductive mediums (air and oil). According to the reference photos, some amount of gas flows on the top of the pipe (operating point P5, Fig. 14a) and only homogenous water-oil dispersion can be observed on P8 (Fig. 14b). As can be noticed, the inverse problem solution produced uncorrected results on both flow conditions, where a large amount of air was wrongly inferred instead of oil. In contrast, the threshold-based method produced visualizations in good agreement with the references for both experiments.

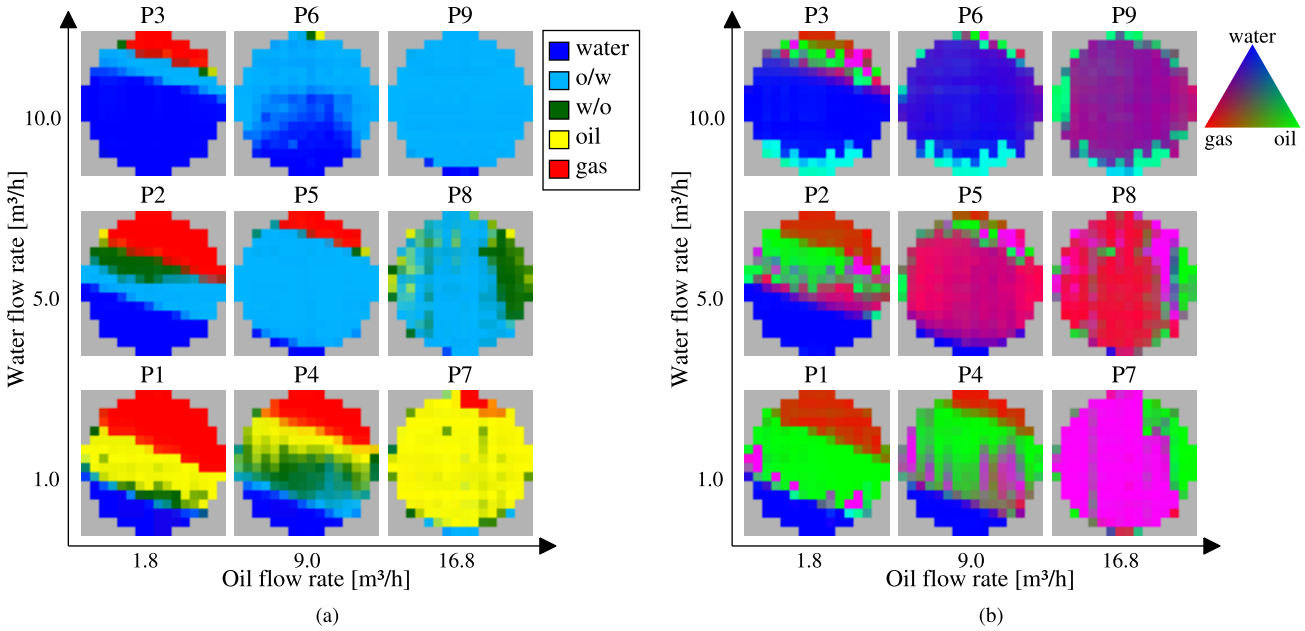

FIGURE 12. Three-phase flow visualization (a) with the proposed threshold-based method, and (b) with the inverse problem solution [27].

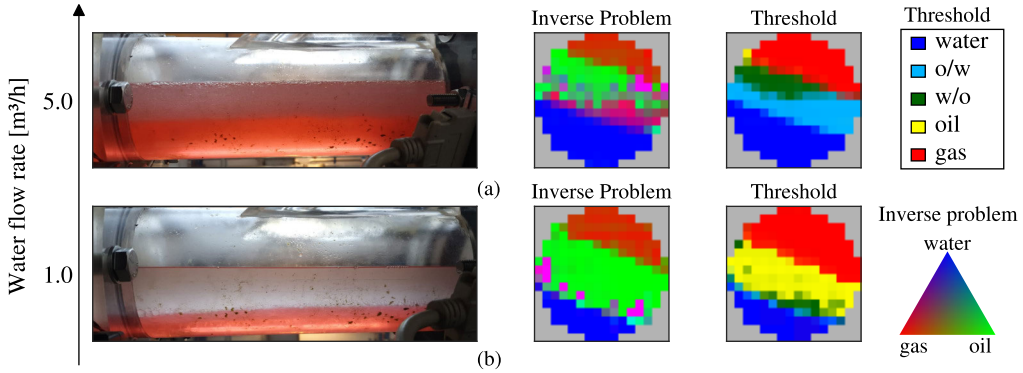

FIGURE 13. Constant oil flow rate 1.8 m^3/h. (a) Experimental data P2; (b) Experimental data P1.

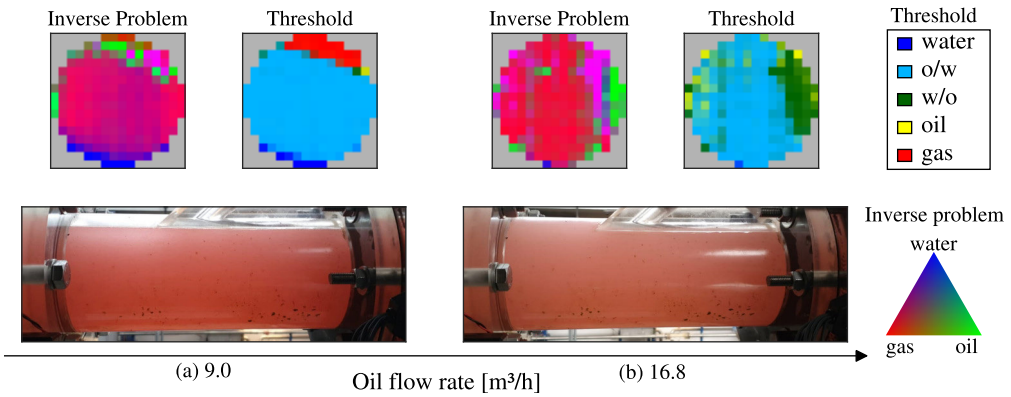

FIGURE 14. Constant water flow rate 5.0 m^3/h. (a) Experimental data P5; (b) Experimental data P8.

C. QUANTITATIVE BOUNDARY EVALUATION OF PHASE FRACTIONS

In addition to imaging capability, the threshold-based method provides the maximum and minimum water-oil and gas phase fractions for each control volume. For convenience, we have divided each phase by liquid fraction. In this way, Fig. 15 relates the average water-in-liquid (Fig. 15a) and gas-in-liquid fraction (Fig. 15b) from 5000 frames estimated

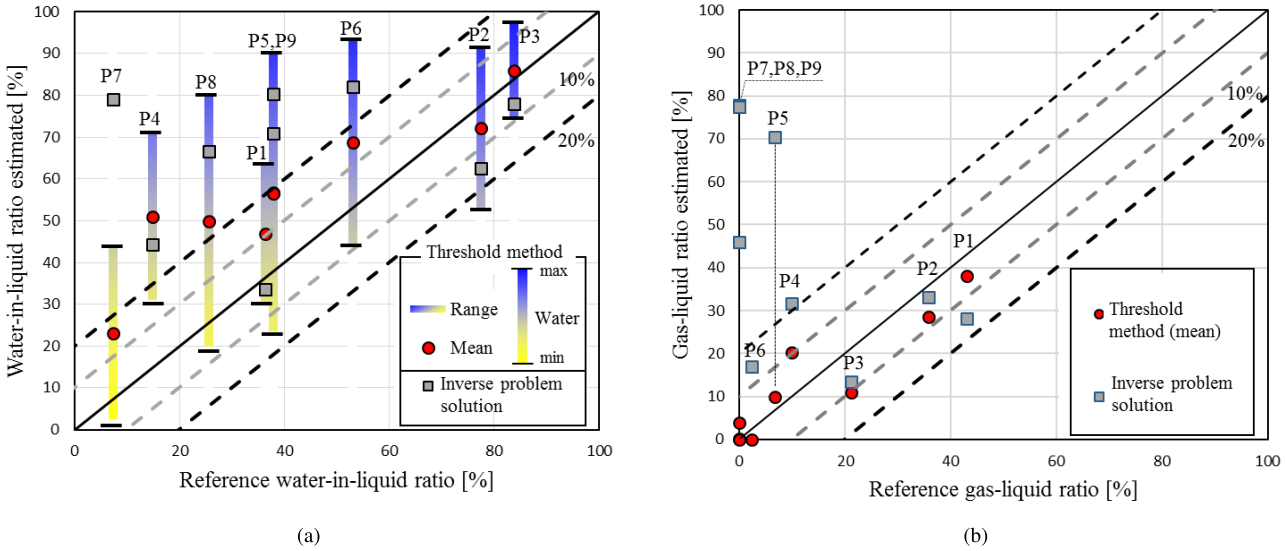

FIGURE 15. Quantitative results of the new threshold-based method and inverse problem solution [26]. (a) Water-in-liquid estimation. The legend scale on right top represents the intervals from Eq. (36) to (39). (b) Gas-in-liquid estimation.

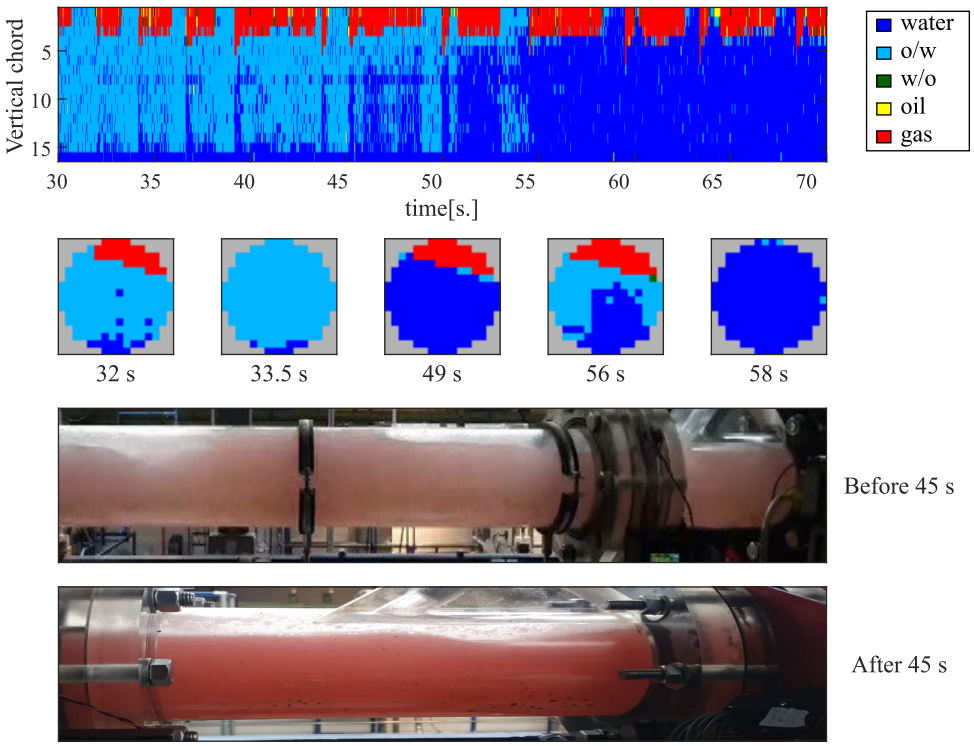

FIGURE 16. Transient three-phase (plug) flow visualization with the threshold method.

using the procedure described in section III-C4. In Fig. 15a, the colour bar represents the possible values in between the boundaries $\overline{\alpha}_x/\overline{\alpha}_{liquid}$, obtained from Eq. (36) to (39). As can be seen, the proposed threshold-based method provided satisfactory results for all operating points. Each interval crosses the reference, which indicates an accurate classification. Although the goal of the proposed method is not to give the exact phase fraction distribution, the mean value of operating points P1, P2 and P3 provided good estimates, with less than 10% deviation. Less than 20% deviation for the other points is also satisfactory. In comparison, the inverse problem also provided good agreement for the same points P1, P2 and P3, but incorrect results for the others.

D. TRANSIENT THREE-PHASE FLOW VISUALIZATION

A final experiment was performed to check the capability of the new threshold-based method to visualize a transient three-phase flow, as detailed following. The input water and oil flow rate were set on 15.90 and 9.22 m^3/h, respectively. In addition, the air was injected downstream the water-oil mixer in order to produce slug flow. This condition was kept up to 45 s. After that, the water flow rate was set to 25.12 m^3/h and oil flow rate to 0 m^3/h to create a transient condition (see Table 4, Experimental point P10). Fig. 16 shows virtual side views of the flow, i.e. the vertical chord of wire-mesh sensor and five selected frames over time. Flow regime may be visually classified as plug flow, with gas bubbles in the top of the pipe. As expected, the new method was able to visualize the dynamics of the flow with high temporal and spatial resolution. It was also capable of sensing changes on the liquid phase. As can be seen in Fig. 16, up to 45 s the mixture is composed mostly of oil-in-water dispersion while air slugs flow on top of the pipe. The transient of the liquid phase starts after 45 s, where the water fraction finally becomes 90% to 100% (see Table 1). This yet simple experiment shows the high potential of dual-modality wire-mesh sensor in order to deal with very fast multiphase flows.

VI. CONCLUSIONS

In this work, we presented a novel threshold-based method for water-oil-air three-phase flow visualization. This method is an alternative to deal with limitations of the inverse problem. The algorithm proposed was validated with experimental data. The electrical properties of the fluid (conductivity and permittivity) were estimated by means of a new dual-modality wire-mesh sensor, where qualitative and quantitative evaluations were performed. The results suggest that the new threshold-based method can be used to visualize water-oil-air three-phase flow even in the presence of water/oil dispersions.

The results presented in this work show the potential of dual-modality wire-mesh sensor to visualize and to quantify the range of individual phase fraction of water-oil-gas three-phase flow. It also suggests that the threshold-based method is much more robust against ambiguities between oil and air components, when compared with the inverse problem formulation presented in [27]. Although the threshold method does not provide the exact phase fraction distribution, it may be achieved in further works by including non-ideal aspects of the measurement system, i.e. electric field nonlinearities and losses.

ACKNOWLEDGMENT

The authors would like to thank the Royal Society, U.K., for awarding the Newton Mobility Grant (NMG\R2\170169) without which the collaboration resulted in producing this article would not have been possible.

REFERENCES

[1] G. Falcone, G. Hewitt, and C. Alimonti, *Multiphase Flow Metering: Principles and Applications*, vol. 54. Amsterdam, The Netherlands: Elsevier, 2009.
[2] L. S. Hansen, S. Pedersen, and P. Durdevic, "Multi-phase flow metering in offshore oil and gas transportation pipelines: Trends and perspectives," *Sensors*, vol. 19, no. 9, p. 2184, May 2019.
[3] R. Thorn, G. A. Johansen, and B. T. Hjertaker, "Three-phase flow measurement in the petroleum industry," *Meas. Sci. Technol.*, vol. 24, no. 1, Jan. 2013, Art. no. 012003.
[4] M. Wang, *Industrial Tomography: Systems and Applications*. Amsterdam, The Netherlands: Elsevier, 2015.
[5] U. Hampel, F. Barthel, M. Bieberle, M. Schubert, and E. Schleicher, "Multiphase flow investigations with ultrafast electron beam X-ray tomography," *AIP Conf. Proc.*, vol. 1428, pp. 167–174, Mar. 2012.
[6] F. Barthel, M. Bieberle, D. Hoppe, M. Banowski, and U. Hampel, "Velocity measurement for two-phase flows based on ultrafast X-ray tomography," *Flow Meas. Instrum.*, vol. 46, pp. 196–203, Dec. 2015.
[7] C. Sátre, G. A. Johansen, and S. A. Tjugum, "Tomographic multiphase flow measurement," *Appl. Radiat. Isot.*, vol. 70, no. 7, pp. 1080–1084, Jul. 2012.
[8] E. M. Bruvik, B. T. Hjertaker, and A. Hallanger, "Gamma-ray tomography applied to hydro-carbon multi-phase sampling and slip measurements," *Flow Meas. Instrum.*, vol. 21, no. 3, pp. 240–248, Sep. 2010.
[9] A. Bieberle, H.-U. Härting, S. Rabha, M. Schubert, and U. Hampel, "Gamma-ray computed tomography for imaging of multiphase flows," *Chem. Ingenieur Technik*, vol. 85, no. 7, pp. 1002–1011, Jul. 2013.
[10] A. Bieberle, H. Nehring, R. Berger, M. Arlit, H.-U. Härting, M. Schubert, and U. Hampel, "Compact high-resolution gamma-ray computed tomography system for multiphase flow studies," *Rev. Sci. Instrum.*, vol. 84, no. 3, Mar. 2013, Art. no. 033106.
[11] Z. Xu, F. Wu, X. Yang, and Y. Li, "Measurement of gas-oil two-phase flow patterns by using CNN algorithm based on dual ECT sensors with venturi tube," *Sensors*, vol. 20, no. 4, p. 1200, Feb. 2020.
[12] A. D. N. Wrasse, T. P. Vendruscolo, E. N. dos Santos, D. R. Pipa, H. L. de Moura, F. C. Castaldo, R. E. M. Morales, and M. J. da Silva, "Capacitive multielectrode direct-imaging sensor for the visualization of two-phase flows," *IEEE Sensors J.*, vol. 17, no. 24, pp. 8047–8058, Dec. 2017.
[13] M. Wang, "Impedance mapping of particulate multiphase flows," *Flow Meas. Instrum.*, vol. 16, nos. 2–3, pp. 183–189, Apr. 2005.
[14] S. Pedersen, C. Mai, L. Hansen, P. Durdevic, and Z. Yang, "Online slug detection in multi-phase transportation pipelines using electrical tomography," *Ifac-Papersonline*, vol. 48, no. 6, pp. 159–164, 2015.
[15] E. Schleicher, M. J. da Silva, S. Thiele, A. Li, E. Wollrab, and U. Hampel, "Design of an optical tomograph for the investigation of single- and two-phase pipe flows," *Meas. Sci. Technol.*, vol. 19, no. 9, Sep. 2008, Art. no. 094006.
[16] N. Zeng, S. Lai, and Y. Liao, "Optical tomography for two-phase flow measurement," in *Proc. Opt. Diag. for Fluids, Solids, Combustion*, Nov. 2001, pp. 341–347.
[17] R. S. Bernardelli, E. N. dos Santos, R. Morales, D. R. Pipa, and M. J. da Silva, "GPU-accelerated simulator for optical tomography applied to two-phase flows," in *Proc. IEEE Int. Conf. Imag. Syst. Techn. (IST)*, Dec. 2019, pp. 1–6.
[18] M. Yang, H. I. Schlaberg, B. S. Hoyle, M. S. Beck, and C. Lenn, "Real-time ultrasound process tomography for two-phase flow imaging using a reduced number of transducers," *IEEE Trans. Ultrason., Ferroelectr., Freq. Control*, vol. 46, no. 3, pp. 492–501, May 1999.
[19] B. Hoyle, "Real-time ultrasound process tomography in pipelines," in *Proc. IEE Colloq. Ultrasound Process Ind.*, 1993, pp. 1–4.
[20] C. Tan, X. Li, H. Liu, and F. Dong, "An ultrasonic transmission/reflection tomography system for industrial multiphase flow imaging," *IEEE Trans. Ind. Electron.*, vol. 66, no. 12, pp. 9539–9548, Dec. 2019.
[21] J. Hitomi, Y. Murai, H. J. Park, and Y. Tasaka, "Ultrasound flow-monitoring and flow-metering of air–oil–water three-layer pipe flows," *IEEE access*, vol. 5, pp. 15021–15029, 2017.
[22] L. D. Hall, "Roles for magnetic resonance imaging in process tomography," *IEEE Sensors J.*, vol. 5, no. 2, pp. 125–133, Apr. 2005.
[23] M. M. Britton, "MRI of chemical reactions and processes," *Prog. Nucl. Magn. Reson. Spectrosc.*, vol. 101, pp. 51–70, Aug. 2017.
[24] H.-M. Prasser, A. Böttger, and J. Zschau, "A new electrode-mesh tomograph for gas–liquid flows," *Flow Meas. Instrum.*, vol. 9, no. 2, pp. 111–119, Jun. 1998.
[25] M. Da Silva, E. Schleicher, and U. Hampel, "Capacitance wire-mesh sensor for fast measurement of phase fraction distributions," *Meas. Sci. Technol.*, vol. 18, no. 7, p. 2245, 2007.
[26] E. N. dos Santos, E. Schleicher, S. Reinecke, U. Hampel, and M. J. Da Silva, "Quantitative cross-sectional measurement of solid concentration distribution in slurries using a wire-mesh sensor," *Meas. Sci. Technol.*, vol. 27, no. 1, Jan. 2016, Art. no. 015301.

[27] E. N. dos Santos, T. P. Vendruscolo, R. E. M. Morales, E. Schleicher, U. Hampel, and M. J. Da Silva, "Dual-modality wire-mesh sensor for the visualization of three-phase flows," *Meas. Sci. Technol.*, vol. 26, no. 10, Oct. 2015, Art. no. 105302.

[28] E. N. dos Santos, M. J. da Silva, R. E. M. Morales, S. Reinecke, E. Schleicher, and U. Hampel, "Dual-modality impedance wire-mesh sensor for investigation of multiphase flows," in *Proc. IEEE Int. Conf. Imag. Syst. Techn. (IST)*, Oct. 2014, pp. 316–319.

[29] Q. Wang, M. Wang, K. Wei, and C. Qiu, "Visualization of gas–oil–water flow in horizontal pipeline using dual-modality electrical tomographic systems," *IEEE Sensors J.*, vol. 17, no. 24, pp. 8146–8156, Dec. 2017.

[30] C. Gunes, Q. M. Marashdeh, and F. L. Teixeira, "A comparison between electrical capacitance tomography and displacement-current phase tomography," *IEEE Sensors J.*, vol. 17, no. 24, pp. 8037–8046, Dec. 2017.

[31] Q. Wang, X. Jia, and M. Wang, "Fuzzy logic based multi-dimensional image fusion for gas–oil-water flows with dual-modality electrical tomography," *IEEE Trans. Instrum. Meas.*, vol. 69, no. 5, pp. 1948–1961, May 2020.

[32] F. D. A. Dias, D. R. Pipa, and M. J. da Silva, "Increasing resolution of wire-mesh sensor data using statistical reconstruction approach," in *Proc. 8th World Congr. Ind. Process Tomograph. (WCIPT)*. Iguassu Falls, Brazil: International Society for Industrial Process Tomography, Sep. 2016, pp. 1–6.

[33] K. Sun and Y. Li, "An HDTV-SB imaging algorithm for wire-mesh tomography," *Meas. Sci. Technol.*, vol. 31, no. 4, Apr. 2020, Art. no. 045404.

[34] S. Ren, H. Liu, C. Tan, and F. Dong, "Tomographic wire-mesh imaging of water-air flow based on sparse minimization," *IEEE Sensors J.*, vol. 17, no. 24, pp. 8187–8195, Dec. 2017.

[35] R. E. Best, *Phase Locked Loops: Design, Simulation, and Applications*. New York, NY, USA: McGraw-Hill, 2007.

[36] M. J. Da Silva, S. Thiele, L. Abdulkareem, B. J. Azzopardi, and U. Hampel, "High-resolution gas–oil two-phase flow visualization with a capacitance wire-mesh sensor," *Flow Meas. Instrum.*, vol. 21, no. 3, pp. 191–197, Sep. 2010.

[37] M. J. da Silva, *Impedance Sensors for Fast Multiphase Flow Measurement and Imaging*. Dresden, Germany: TUDpress, 2008.

[38] R. Thorn, G. A. Johansen, and E. A. Hammer, "Recent developments in three-phase flow measurement," *Meas. Sci. Technol.*, vol. 8, no. 7, pp. 691–701, Jul. 1997.

[39] O. Pekonen, K. Kärkkäinen, A. Sihvola, and K. Nikoskinen, "Numerical testing of dielectric mixing rules by fdtd method," *J. Electromagn. Waves Appl.*, vol. 13, no. 1, pp. 67–87, Jan. 1999.

[40] A. Abou-Arkoub, R. Thorn, and A. Bousbaine, "Online validation of multiphase flowmeters using simple capacitance sensors," *IEEE Trans. Instrum. Meas.*, vol. 59, no. 10, pp. 2671–2682, Oct. 2010.

[41] M. J. Da Silva, E. N. dos Santos, U. Hampel, I. H. Rodriguez, and O. M. H. Rodriguez, "Phase fraction distribution measurement of oil–water flow using a capacitance wire-mesh sensor," *Meas. Sci. Technol.*, vol. 22, no. 10, Oct. 2011, Art. no. 104020.

[42] H.-M. Prasser and R. Häfeli, "Signal response of wire-mesh sensors to an idealized bubbly flow," *Nucl. Eng. Design*, vol. 336, pp. 3–14, Sep. 2018.

[43] L. Van Beek, "Dielectric behaviour of heterogeneous systems," *Prog. Dielect.*, vol. 7, no. 71, p. 113, 1967.

[44] E. Dykesteen, A. Hallanger, E. A. Hammer, E. Samnoy, and R. Thorn, "Non-intrusive three-component ratio measurement using an impedance sensor," *J. Phys. E, Sci. Instrum.*, vol. 18, no. 6, p. 540, 1985.

[45] H.-M. Prasser, E. Krepper, and D. Lucas, "Evolution of the two-phase flow in a vertical tube—Decomposition of gas fraction profiles according to bubble size classes using wire-mesh sensors," *Int. J. Thermal Sci.*, vol. 41, no. 1, pp. 17–28, 2002.

[46] E. Komonibo, "Liquid-liquid flow in baffled vessels and pipes," Ph.D. dissertation, Dept. Chem. Environ. Eng., Univ. Nottingham, Nottingham, U.K., 2018. [Online]. Available: http://eprints.nottingham.ac.uk/id/eprint/49135

[47] F. D. A. Dias, E. N. Dos Santos, M. J. Da Silva, E. Schleicher, R. E. M. Morales, B. Hewakandamby, U. Hampel, "New algorithm to discriminate phase distribution of gas-oil-water pipe flow with dual-modality wire-mesh sensor—Data set [data set]," Rodare, Data Set, 2020, doi: 10.14278/rodare.373.

[48] *Image Processing Toolbox: User's Guide*, MathWorks, Natick, MA, USA, 2018. [Online]. Available: https://de.mathworks.com/help/pdf_doc/images/images_ug.pdf

FELIPE D. A. DIAS received the B.Sc. degree in mechatronic engineering from the Federal Center for Technological Education of Minas Gerais, Divinópolis, Brazil, in 2015, and the M.Sc. degree in electrical engineering with expertise in automation and systems from the Federal University of Technology-Paraná, Curitiba, Brazil, in 2017. He is currently pursuing the Ph.D. degree with the Dresden University of Technology, Dresden, Germany. Since 2017, he has been a Research Associate with Helmholtz-Zentrum Dresden-Rossendorf, Dresden. His current research interests include numerical simulation, modeling, data processing, and design/optimization of industrial sensors.

EDUARDO N. DOS SANTOS (Member, IEEE) received the bachelor's degree in computer engineering from Universidade Positivo, Curitiba, Brazil, in 2009, and the M.Sc. and D.Sc. degrees in electrical engineering with expertise in automation and systems engineering from the Federal University of Technology-Paraná, Brazil, in 2011 and 2015, respectively. He was a Research Assistant with Helmholtz-Zentrum Dresden-Rossendorf, Dresden, in 2014. He is currently a Postdoctoral Researcher with the Multiphase Flow Research Center (NUEM). His current research interests include sensing technology, data processing, and development of instrumentation and sensors applied to process monitoring.

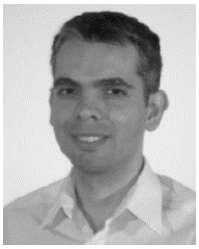

MARCO J. DA SILVA (Senior Member, IEEE) received the M.Sc. degree in electrical engineering from the Dresden University of Technology, Dresden, Germany, and the Federal University of Technology-Paraná, Curitiba, Brazil, in 2003, and the Dr.-Ing. degree in electrical engineering from the Dresden University of Technology, in 2008. He was a Research Associate with Helmholtz-Zentrum Dresden-Rossendorf, Dresden, from 2004 to 2009. In 2010, he joined the Federal University of Technology-Paraná, where he has been an Associate Professor, since 2013. His current research interests include sensing technology, sensor data processing, and instrumentation applied to process monitoring. He is a Topical Editor of the IEEE Sensors Journal. He is on the Editorial Board of *Measurement Science and Technology*.

ECKHARD SCHLEICHER received the Diploma degree in electrical engineering from the Dresden University of Technology, in 1998. He worked as a Research Associate with the Institute of Biomedical Engineering, Dresden University of Technology, on the research topics of diffuse optical tomography and tissue optical spectroscopy, until 1999. From 1999 to 2002, he worked as a Ph.D. student with the Optical Diagnostics Research Group, Institute of Biomedical Engineering, Faculty of Electrical Engineering, Dresden University of Technology, on the research topics of tissue and radio-frequency laser spectroscopy. Since 2003, he has been a Research Associate with Helmholtz-Zentrum Dresden-Rossendorf e.V., Institute of Fluid Dynamics, on the development and novel methods for multiphase-flow measurement and visualization in process diagnostics. His research interests are conductivity and capacitance based wire-mesh sensors and needle probe systems, gamma ray tomography, ultra-fast X-ray computed tomography, and optical tomography.

RIGOBERTO E. M. MORALES received the B.S. degree in fluid mechanical engineering from the National University of San Marcos, Lima, Peru, in 1993, the M.Sc. degree in mechanical engineering from the Federal University of Uberlândia, Uberlândia, Brazil, in 1996, and the Ph.D. degree in mechanical engineering from the University of Campinas, Campinas, Brazil, in 2000. He is currently a Professor with the Mechanical Engineering Department, Federal University of Technology-Paraná, Curitiba, Brazil. His current research interests include mathematical modeling, numerical simulation, and experimentation for multiphase flows.

BUDDHIKA HEWAKANDAMBY received the Ph.D. degree in chemical engineering from the University of Sheffield, Sheffield, U.K., in 2002. He is currently an Associate Professor with the Department of Chemical and Environmental Engineering, University of Nottingham, Nottingham, U.K. His current research interests are in the area of fluid dynamics, including multiphase flows, microfluidics, and heat and mass transfer in multiphase flows. He is a member of the Institute of Physics and also an Associate Member of IChemE.

UWE HAMPEL was born in Zwickau, Germany, in 1968. He received the Diploma degree in computer science from the Technische Universität Dresden, Germany, in 1993, the M.Sc. degree in digital systems engineering from Heriot–Watt University, Edinburgh, U.K., the Ph.D. and Habilitation degrees from the Technische Universität Dresden, in 1998 and 2005, respectively. Since 2006, he has been the Head of the Experimental Thermal Fluid Dynamics Division, Helmholtz-Zentrum Dresden-Rossendorf, Germany, and since 2012 a Professor of imaging techniques for energy and process engineering with Technische Universität Dresden. He was awarded the title of Doctor honoris causa at the University of Liége, in 2019. His research interests are flow measurement techniques, process tomography, and multiphase flow.